Available online at www.sciencedirect.com
SCIENCE DIRECT®
Journal of Nuclear Materials 346 (2005) 131–144
journal of nuclear materials
www.elsevier.com/locate/jnucmat

Matrix swelling rate and cavity volume balance of UO_2 fuels at high burn-up

J. Spino [a,*], J. Rest [b], W. Goll [c], C.T. Walker [a]

[a] European Commission, Joint Research Centre, Institute for Transuranium Elements, P.O. Box 2340, D-76125 Karlsruhe, Germany
[b] Argonne National Laboratory, Energy Technology 212, 9700 S. Cass Avenue, Argonne, IL 60439-4815, USA
[c] FRAMATOME ANP GmbH, Freyeslebenstr. 1, Postfach 3220, 91050 Erlangen, Germany

Received 25 February 2005; accepted 10 June 2005

Abstract

The low temperature matrix swelling of UO_2 fuels was analysed as a function of burn-up, taking into account changes in the fuel density, porosity and retained Xe concentration as measured by EPMA. The evaluation of these data combined with an analytical solution to a rate-theory model for gas-driven swelling leads to the conclusion that at average pellet burn-ups $\leqslant$ 60 GWd/t M the total matrix swelling rate is gradually reduced from $\approx$1% per 10 GWd/t M to $\approx$0.3% per 10 GWd/t M; the latter value being reached at an average burn-up above 110 GWd/t M. The decrease in the swelling rate is due to the progressive depletion of fission gas in the fuel matrix by thermal and athermal processes, such that at very high burn-up the matrix swelling becomes dominated by the precipitation of solid fission products. Owing to volume conservation, the volume occupied by the depleted gas is replaced by porosity.

1. Introduction

The volume change of the active column of nuclear fuels during service in the reactor is a fact that was recognized in the early irradiation experiments [1]. Because of its impact on vital aspects of fuel performance such as heat transfer at the fuel-cladding gap (gap closure) and cladding strain, this issue has repeatedly drawn the attention of nuclear fuel designers and engineers over the years.

At large exposures the effect is dominated by the fuel swelling driven by the precipitation of the insoluble fission products in the fuel matrix, which in either solid or gaseous state require more space than the precursor U-atoms. Insoluble solid fission products that segregate in the form of metallic or oxide inclusions, or noble fission gas atoms that remain trapped in the fuel matrix, are associated with atomic volumes that vary respectively between 1.3 and 2 times that of the U atoms in the host UO_2 lattice [2,3]. A macroscopic volume expansion during the irradiation is therefore inevitable. Soluble fission products cause only slight modifications of the lattice volume [3,4].

Under low temperature conditions where thermal migration of gases and bubble growth and coalescence processes are negligible, this fuel expansion constitutes the so-called 'solid or inexorable swelling' [5,6], which represents the volume increase of the fuel that only depends on burn-up and that cannot be suppressed or

* Corresponding author. Tel.: +49 7247 951233; fax: +49 7247 951590.
E-mail address: jose.spino@itu.fzk.de (J. Spino).

0022-3115/$ - see front matter © 2005 Elsevier B.V. All rights reserved.
doi:10.1016/j.jnucmat.2005.06.015

mitigated by the application of external pressure. Our purpose in this paper is to quantify the evolution of this term at high burn-up, and to elucidate how it matches with the evolution of porosity, particularly in view of the considerable porosity increase during the formation of the rim structure [7].

The analysis considers experimental data from LWR-fuels irradiated to an average burn-up of about 100 GWd/tM. It is worth noting that in a previous review by Schrire et al. [6] of irradiation data limited to average fuel burn-up of 65 GWd/tM, the authors suggested a decrease of the inexorable swelling at the highest burn-up, presumably due to fission gas precipitation into large bubbles. In the present work, we confirm this trend, with onset at burn-ups around 60 GWd/tM.

2. Definition of terms

Swelling is defined as the fractional increase of the bulk fuel volume at a given burn-up with respect to its value at the beginning of the irradiation. Under closed system conditions (mass conservation) this is expressed as [3]:

$$\Delta V^{\text{bulk}}/V_0^{\text{bulk}} = (V^{\text{bulk}} - V_0^{\text{bulk}})/V_0^{\text{bulk}}, \tag{1}$$

where V_0^{bulk} and V^{bulk} are, respectively, the initial and final bulk volumes.

In the presence of porosity the volume terms are replaced by $V_0^{\text{bulk}} = V_0^{\text{matrix}}/(1-P_0)$ and $V^{\text{bulk}} = V^{\text{matrix}}/(1-P)$, where V_0^{matrix} and V^{matrix} are, respectively, the initial and final matrix volumes and P_0 and P the initial and final porosities. Eq. (1) thus takes the general form:

$$\Delta V^{\text{bulk}}/V_0^{\text{bulk}} = (\Delta V^{\text{matrix}}/V_0^{\text{matrix}})(1-P_0)/(1-P) + (P-P_0)/(1-P), \tag{2}$$

where $\Delta V^{\text{matrix}}/V_0^{\text{matrix}}$ represents the fuel matrix swelling split into the contributions of solid and gaseous fission products, i.e, $\Delta V^{\text{solid FP}}/V_0^{\text{matrix}}$ and $\Delta V^{\text{gaseous FP}}/V_0^{\text{matrix}}$, respectively. In the absence of porosity variations ($P = P_0$), this term is obviously equal to the bulk volume variation.

If the reference state is taken at the beginning of the irradiation where the initial fuel density is given by $\rho_0 = (1-P_0)\rho_{\text{th}}$, ρ_{th} being the theoretical density of UO_2 (10.96 g/cm^3), rearrangement of the terms in Eq. (2) leads to the relationship:

$$\rho/\rho_{\text{th}} = (1-P)/(1+\Delta V^{\text{matrix}}/V_0^{\text{matrix}}), \tag{3}$$

where ρ is the bulk fuel density (ρ can be measured, e.g., by immersion techniques). For small values of P and $\Delta V^{\text{matrix}}/V_0^{\text{matrix}}$ (e.g., $\leqslant 0.12$) Eq. (3) can be closely approximated by:

$$\rho/\rho_{\text{th}} \cong 1 - P - \Delta V^{\text{matrix}}/V_0^{\text{matrix}}. \tag{4}$$

Though only approximate, Eq. (4) allows the reader to easily visualize the key volume balance in the fuel at a given burn-up, namely showing the connection between the total matrix swelling and the experimentally determined quantities ρ and P.

3. Predicted matrix swelling contributions

3.1. Solid fission products

The term $\Delta V^{\text{solid FP}}/V_0^{\text{matrix}}$ has been evaluated in [2,3] on the basis of the partial volume requirements of the insoluble solid fission products, assuming that they precipitate either as five-metals inclusions (Mo, Ru, Tc, Rh, Pd), or alkaline earth oxides of the type $BaZrO_3$, or compounds of the type Cs(Rb)I, $Cs(Rb)_2Te$, and $Cs(Rb)_2O$. This evaluation results in a volume demand per fission of 1.324 times the volume of the precursor U in the UO_2 lattice [2,3]. This leads to the value 0.32% per 10 GWd/tM that has been assigned historically to the matrix swelling caused by solid fission products.

A direct measurement of the above quantity or a more refined calculation of it does not exist. As regards its fluctuation range, variations in the composition and concentration of the precipitates along the fuel radius, partitioning of elements between the second phases and variations of the oxygen stoichiometry of the fuel matrix, would make necessary to consider a band of values between 0.15% and 0.45% per 10 GWd/tM [3].

3.2. Gaseous fission products

The estimation of the matrix swelling by retained fission gases has been done historically by assuming these gases to precipitate as bubbles in the fuel, under validity of Van der Waals gas conditions [3,5]. As an illustration, for the major gas Xe precipitated in equilibrium bubbles of radius $\leqslant 1$ nm, with the internal pressure dictated by $p_{\text{eq}} = 2\gamma/r$ (γ = solid surface energy, r = bubble radius, $\gamma_{UO2} \sim 1$ J/m^2 [3]), the assumption of Van der Waals conditions leads to a molecular volume of 8.5×10^{-23} cm^3/atom [3]. This doubles the molecular volume of solid UO_2, which is approximately equal to 4.1×10^{-23} cm^3/atom [3].

The fractional volume increase of the fuel by retained fission gases (Xe) may be expressed as:

$$\Delta V^{\text{gaseous FP}}/V_0^{\text{matrix}} = N_{\text{Xe}} \cdot v_{\text{Xe}}, \tag{5}$$

where N_{Xe} is the total volume concentration of Xe atoms and v_{Xe} is the volume occupied by these atoms in UO_2, with N_{Xe} being given by $N_{\text{Xe}} = F \cdot Y_{\text{Xe}} \cdot BU$, where F is the fission density per unit burn-up, Y_{Xe} is the Xe-yield and BU is the burn-up in GWd/tM. Thus, by virtue of Eq. (5) and with the molecular volume above, for each

10 GWd/tM, a fractional volume increase by fission gases of 0.0056 cm^3/cm^3 is calculated, which is equivalent to a matrix-swelling rate of 0.56% per 10 GWd/tM. (Assumptions: $F = 2.53 \times 10^{19}$ fissions/cm^3 per GWd/t M, given an energy release per fission of 200 MeV ($=3.2 \times 10^{-11}$ W s); $Y_{Xe} = 0.26$, considering the increased contribution of ^{239}Pu fissions at high burn-ups.)

Since when added to the average contribution of solid fission products (0.32% per 10 GWd/tM), this gas swelling rate leads to a total inexorable swelling that falls within the range of experimental values (0.8–1% per 10 GWd/tM for burn-ups $\leqslant$40 GWd/tM [5,8–11]), the above formulation has found wide acceptance in the field [5,6]. As a further refinement, for parts of the fuel experiencing gas release, it has been proposed that the so-calculated swelling should be decreased by an amount equivalent to 8.5×10^{-23} cm^3 for every gas atom released from the matrix [5].

However, not all the gas present in the fuel matrix is in form of bubbles, nor is the density of the gas in <1 nm-bubbles well predicted by the Van der Waals equation of state (EOS). Indeed, the application of Ronchi's more exact hard-sphere model (HS)-EOS for Xe [12] for the pressure range expected in 1 nm-equilibrium-bubbles in UO_2 fuels ($p_{eq} \approx 2$ GPa, $T \approx 700$–1400 K), leads to a molecular volume for Xe of 5.3–6.0×10^{-23} cm^3/atom. This implies 29–38% lower fuel swelling than that calculated with the Van der Waal's EOS. In addition, due to fission-induced re-solution a large part of the gas in bubbles is re-injected into the lattice and is kept in dynamic solution [3]. Therefore, a theoretical model was developed to more realistically estimate the variation of these quantities with burn-up, including the partitioning of the bubble-swelling into intragranular and intergranular components. This model is described in Section 3.3.

3.3. Analytical estimate of the fission-gas-induced swelling rate

The model presented in this section considers analytical solutions to coupled rate equations that describe the nucleation and growth of inter- and intragranular bubbles under the simultaneous effect of irradiation-induced gas-atom re-solution. The goal of the formulation is to avoid a coupled set of nonlinear equations that can only be solved numerically, using instead simplified, physically reasonable hypothesis that make the analytical solutions viable. The gas-induced swelling rate is then assessed by calculating the evolution of the bubble population with burn-up and subsequently the amounts of gas in bubbles and lattice sites. Parameters of the model are adjusted by fitting the calculated bubble populations at given burn-ups with measured bubble size and density data.

At the irradiation temperatures of interest ($T <$ 1200 K), the diffusion of fission gas atoms is athermal and proportional to the fission rate, $\dot{f}$ (fissions $\cdot$ $cm^{-3}s^{-1}$), with $\int_0^t \dot{f}\,dt = \int_0^{BU(t)} F\,dBU$ where F and BU are as defined in Section 3.2, and is given by

$$D_g = D_0 \dot{f}. \tag{6}$$

In general, the gas-atom re-solution rate is also proportional to the fission rate, i.e.,

$$b = b_0 \dot{f}. \tag{7}$$

The rate equation describing the time evolution of the density of gas in intragranular bubbles is given by

$$\frac{d[n_b(t)c_b(t)]}{dt} = 16\pi f_n D_g r_g c_g(t) c_g(t) + 4\pi r_b(t) D_g c_g(t) c_b(t) - b n_b(t) c_b(t). \tag{8}$$

The three terms on the right hand side of Eq. (8) represent, respectively, the change in the density of gas in intragranular bubbles due to bubble nucleation, the gas-atom diffusion to bubbles of radius r_b, and the loss of gas atoms from bubbles due to irradiation induced re-solution. Eq. (8) can also be represented as the sum of two equations denoting, respectively, the time evolution of the fission gas bubble density, c_b, and of the gas content in bubbles, n_b, as follows:

$$\frac{dc_b(t)}{dt} = \frac{16\pi f_n D_g r_g c_g(t) c_g(t)}{n_b(t)} - \frac{b}{2} c_b(t) \tag{9}$$

$$\frac{dn_b}{dt} = 4\pi r_b(t) D_g c_g(t) - \frac{b}{2} n_b(t) \tag{10}$$

In Eq. (9) f_n is the bubble nucleation factor, and c_g and r_g are the gas atom concentration and radius, respectively. In general, the value of f_n is less than one reflecting the premise that gas-bubble nucleation within the UO_2 matrix requires the presence of vacancies/vacancy clusters in order to become viable. The value of f_n was first estimated based on the hypothesis that bubble nucleation is a heterogeneous process and occurs predominantly along fission tracks. In this case f_n is approximately the fractional volume of fission tracks (i.e., $\approx 10^{-4}$) [13].

The first term on the right hand side (rhs) of Eq. (9) can be interpreted to represent the generation rate of 'average' size bubbles of radius r_b. For every 2 atom bubble that is nucleated, $2/n_b$ of a bubble of radius r_b appears. In other words, nucleation of n_b two-atom clusters leads to the gain of one bubble of radius r_b. This 'average size' bubble is in the peak region of the bubble-size distribution [14,15].

Both 'whole' bubble destruction and gas-atom 'chipping' from bubbles are included (last terms on rhs) in Eqs. (9) and (10) in order to capture the behaviour of an average size bubble (that characterizes the full bubble-size distribution). Within the full bubble-size

distribution there are bubbles that are destroyed by one fission fragment collision (e.g., bubbles smaller than a critical size) and others that are only partially damaged (e.g., bubbles larger than a critical size). Including b in both Eqs (9) and (10) is an attempt to depict these processes using a simplified formulation that enables an analytical solution for swelling. If $bc_b/2$ was not included in Eq. (9), then the density of bubbles could never decrease due to irradiation. Likewise if $bn_b/2$ was not included in Eq. (10), the number of atoms in a bubble could never decrease. However, the equal partition of gas-atom re-solution between these two mechanisms, as implied from the use of same re-solution parameter b in Eqs. (9) and (10), is an assumption that remains to be tested experimentally.

Due to the strong effect of irradiation-induced gas-atom re-solution, in the absence of geometric contact, the bubbles stay in the nanometer size range. The density of bubbles increases rapidly early in the irradiation. Subsequently, at longer times, the increase in bubble concentration occurs at a much-reduced rate. Based on the above considerations, the left-hand side of Eq. (9) is set equal to zero. This approximation will be more reasonable for larger values of t. A solution for c_b in terms of n_b and c_g is then given by

$$c_b = \frac{16\pi f_n r_g D_0 c_g^2}{b_0 n_b(t)}. \tag{11}$$

The quantities c_g, c_b and n_b in Eqs. (8)–(11) represent average values. For example, $c_b(t)$ bubbles each containing $n_b(t)$ gas atoms represents the average value of the bubble size distribution at time t. In general, r_b is related to n_b through the gas law and the capillarity relation. Using a modified Van der Waals gas law,

$$\frac{2\gamma}{r_b}\left(\frac{4}{3}\pi r_b^3 - h_s b_v n_b\right) = n_b kT, \tag{12}$$

where γ is the surface tension, b_v is the Van der Waals constant for Xe, k is Boltzmann's constant, T is the absolute temperature, and h_s is a fitting parameter that for a given T makes Eq. (12) equivalent to the hard-sphere equation of state [12].

For bubbles in the nanometer size range an approximate solution to Eq. (12) is given by

$$r_b(t) = \left(\frac{3h_s b_v n_b(t)}{4\pi}\right)^{1/3}. \tag{13}$$

Using Eq. (13) and an argument similar to that used to derive Eq. (11), the steady-state solution to Eq. (10) is given by

$$n_b(t) = \left(\frac{3h_s b_v}{4\pi}\right)^{1/2}\left(\frac{4\pi D_0 c_g(t)}{b_0}\right)^{3/2}. \tag{14}$$

According to Speight [16], the fraction of gas, f_s, that diffuses to the grain boundary of grains of diameter d_g can be approximated by

$$f_s = \frac{8}{d_g}\left(\frac{D_g t}{\pi}\right)^{1/2} - \frac{6}{d_g^2} D_g t. \tag{15}$$

Imposing gas-atom conservation, i.e., requiring that the sum of the gas in solution, in intragranular bubbles, and on the grain boundary is equal to the amount of gas generated, the term $c_g(t)$ is determined as

$$c_g(t) = \frac{-(1+f_s) + [(1+f_s)^2 + 64\pi f_n r_g D_g \dot{f}\,\beta t/b]^{1/2}}{32\pi f_n r_g D_g/b}, \tag{16}$$

where β is the number of gas atoms produced per fission event.

Following the work of Wood and Kear [17], grain boundary bubble nuclei of radius R_b are produced until such time that a gas atom is more likely to be captured by an existing nucleus than to meet another gas atom and form a new nucleus. An approximate result for the grain-boundary bubble concentration is given by

$$C_b = \left(\frac{8zaK}{12^{1/3}\pi^2 \xi D_g \delta}\right)^{1/2}, \tag{17}$$

where $\frac{a^3}{12}$ is the average atomic volume in UO_2 [18], a is the lattice constant, z is the number of sites explored per gas-atom jump, δ is the width of the boundary, ξ is a grain-boundary diffusion enhancement factor, and K is the flux of gas-atoms per unit area of grain boundary.

The intergranular bubble nucleation and growth formulation incorporated here is based on the assumption that, although the effect of radiation-induced re-solution on intergranular bubble behavior is not negligible, a reasonable approximation can be obtained by neglecting such effect in the governing equations [19].

Under the above considerations, the flux K of atoms at the grain boundary is given by

$$K = \frac{d_g}{3}\frac{dc_g}{dt}\frac{d(f_s t)}{dt}. \tag{18}$$

Differentiating Eq. (16)

$$\frac{dc_g}{dt} = \frac{\beta \dot{f} - c_g df_s/dt}{(1 + f_s + 32\pi f_n r_g D_g c_g/b)}, \tag{19}$$

where, using Eq. (15)

$$\frac{d(f_s t)}{dt} = \frac{12}{d_g}\left(\sqrt{\frac{D_g t}{\pi}} - \frac{D_g t}{d_g}\right). \tag{20}$$

The concentration of gas on the grain boundaries, C_g, is given by

$$C_g(t) = \frac{d_g}{3} f_s(t) c_g(t) \tag{21}$$

and the average number of gas atoms in a grain boundary bubble is

$$N_b(t) = \frac{C_g(t)}{C_b(t)}. \quad (22)$$

The radius of a grain boundary bubble is obtained from the solution to Eq. (12), i.e.

$$R_b = \left[\frac{3h_s b_v N_b}{8\pi} + \sqrt{\left(\frac{3h_s b_v N_b}{8\pi}\right)^2 - \left(\frac{N_b kT}{8\pi\gamma}\right)^3}\right]^{1/3} + \left[\frac{3h_s b_v N_b}{8\pi} - \sqrt{\left(\frac{3h_s b_v N_b}{8\pi}\right)^2 - \left(\frac{N_b kT}{8\pi\gamma}\right)^3}\right]^{1/3}. \quad (23)$$

The fractional swelling due to fission gas is thus given by

$$\left(\frac{\Delta V}{V}\right)_g = \frac{c_g a^3}{4} + \frac{4\pi}{3}\left(r_b^3 c_b + R_b^3 C_b\right), \quad (24)$$

where the first term at the right-hand-side of Eq. (24) accounts for the contribution of the gas in dynamic solution, and the second term for the contributions of both intragranular and intergranular bubbles, respectively.

Regarding the gas in dynamic solution, the hypothesis has been made following Matzke [20,21] that gas atoms in the UO_2 lattice become effectively bound to the so-called Schottky trios, i.e., electrically neutral defect complexes consisting of one uranium vacancy and two oxygen vacancies. Thus, corresponding to the ad-atoms on surfaces associated with the Schottky defects [18], for every bound Xe atom (i.e., every atom in dynamic solution) a bulk volume increase of 3 atomic volumes was considered. Since, as mentioned above, the average atomic volume in UO_2 is given approximately by $a^3/12$ ($a = UO_2$ lattice constant) [18], the volume increment assigned per trapped Xe atom is around 4.1×10^{-23} cm^3/atom. This volume is certainly much smaller than that occupied by Xe atoms in bubbles, as calculated both under Van der Waals (8.5×10^{-23} cm^3/atom) or HS-EOS ($5.3–6.0 \times 10^{-23}$ cm^3/atom) conditions (see Section 3.2).

Finally, the fraction of gas in dynamic solution is given by

$$X(t) = \frac{c_g(t)}{c_g(t) + C_g(t) + n_b(t)c_b(t)}. \quad (25)$$

Table 1
Values of parameters used in the calculations

Parameter	Value	References
β	0.25	Olander [3]
ξ	1.65×10^3	This work
b_0	10^{-23} m^3	Marlow and Kaznoff [22]
D_0	1.2×10^{-39} m^5	Matzke [23]
r_g	0.216 nm	Olander [3]
γ	1 J m^{-2}	Olander [3]
b_v	8.5×10^{-29} m^3/atom	Olander [3]
f_n	10^{-2}	This work
h_s	0.6	This work

The values of the key parameters used in the model are given in Table 1. Most of them are known from Refs. [3,22,23]; the values of the others (ξ and f_n) resulted from the fitting of the present theory with measured data of bubble populations [13,24,25]. Table 2 shows thus a comparison between the theory and bubble density and size data. Although the calculated intragranular bubble-size and density are in reasonable agreement with the measured results, no intergranular data is available for comparison with the calculated quantities shown in Table 2. As indicated in Fig. 1, the model calculations show that at the irradiation temperatures of interest ($T < 1200$ K) the fraction of the generated gas residing in bubbles (intragranular + intergranular) increases rapidly early in the irradiation, and much more slowly at extended times (burn-ups). The same occurs with the fraction of gas in intragranular bubbles. However, the latter shows saturation at burn-ups of 20 GWd/tM and even below (Fig. 1). As also shown in Fig. 1, in concert with the increase with burn-up of the total fraction of gas in bubbles, the fraction of the generated gas in dynamic solution, Eq. (25), is found to diminish with time (burn-up), moving from values around 0.8–1 at burn-ups below 5 GWd/tM to values below 0.4 at burn-ups above 23 GWd/tM.

Fig. 2 shows the variation with burn-up of the resulting total matrix-gas swelling, as well as the swelling contributions from gas in dynamic solution and gas in intragranular and intergranular bubbles. The calculated total matrix-gas swelling continuously increases with

Table 2
Comparison between theory and measured data

Burn-up (GWd/tM)	Gas bubble radius (m)			Gas bubble density			References
	Measured (matrix)	Calculated (matrix)	Calculated (grain boundary)	Measured (matrix) (m^{-3})	Calculated (matrix) (m^{-3})	Calculated (grain boundary) (m^{-2})	
6.5	8×10^{-10}	6.9×10^{-10}	1.2×10^{-8}	3.3×10^{23}	3.2×10^{23}	1.7×10^{14}	[13]
8	8.7×10^{-10}	7.4×10^{-10}	1.3×10^{-8}	2.2×10^{23}	3.5×10^{23}	1.7×10^{14}	
13	8.5×10^{-10}	8.9×10^{-10}	1.8×10^{-8}	3.4×10^{23}	4.2×10^{23}	1.7×10^{14}	
23	1.1×10^{-9}	1.1×10^{-9}	2.5×10^{-8}	9×10^{23}	5.1×10^{23}	1.6×10^{14}	[24]
49	3.5×10^{-9}	1.4×10^{-9}	3.9×10^{-8}	5.4×10^{23}	6.5×10^{23}	1.46×10^{14}	[25]

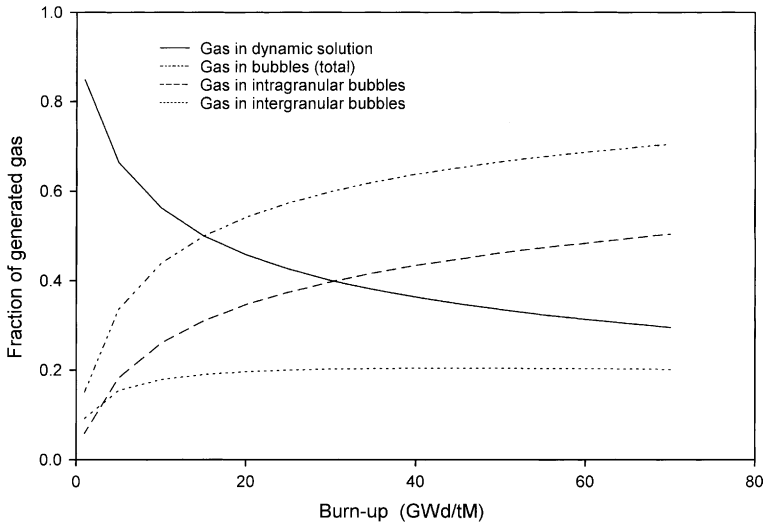

Fig. 1. Variation with burn-up of the fractions of gas in dynamic solution and in intra-granular and intergranular bubbles as calculated from Eq. (25).

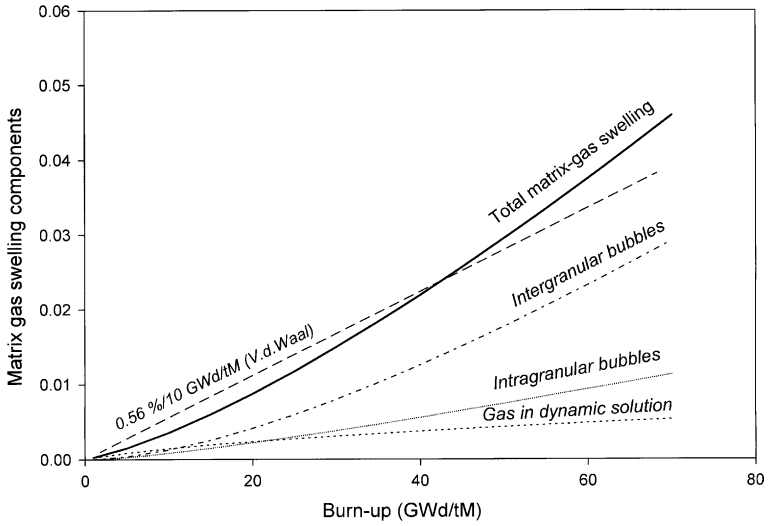

Fig. 2. Variation with burn-up of the total matrix-gas swelling as calculated from the fractions of gas in dynamic solution and in intragranular and intergranular bubbles according to Fig. 1.

burn-up, with increasing slope ranging from ~0.36% per 10 GWd/tM at 10 GWd/tM to 0.7% per 10 GWd/tM at 80 GWd/tM. These swelling rates bound the value of 0.56% per 10 GWd/tM (Fig. 2), which was derived in Section 3.2 by assuming Van der Waals gas conditions and disregarding the effects of gas-atom re-solution and intergranular bubble swelling. Thus, as shown in Fig. 3, adding the solid fission product swelling to the fission gas swelling calculated with the present model leads to total matrix swelling values that match the experimental results in a wide range of burn-ups ($\leqslant$70 GWd/tM).

The agreement obtained using the model described in this section (e.g., Eq. (24)) with experimental swelling data is due, in part, to the important contribution of the intergranular bubble swelling, which for burn-ups above $\approx$30 GWd/tM is larger than the sum of the intragranular bubble swelling plus the contribution of the gas in dynamic solution (Fig. 2). This contribution depends on the value of ξ (see Eq. (17) and Table 1), which is a grain-boundary gas-atom diffusion enhancement factor that reflects the fact that grain boundary diffusion is decidedly faster than grain lattice diffusion [26]. The effect of ξ on the intergranular bubble nucleation is visible

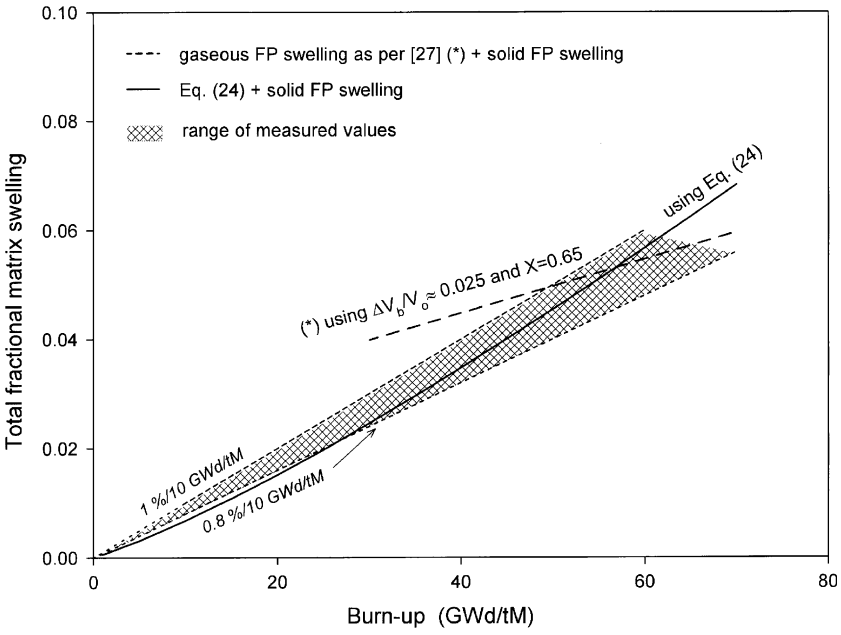

Fig. 3. Total matrix swelling values derived from the present model (Eq. (24)) and from Ref. [27], after adding the contribution of solid fission product swelling (0.32% per 10 GWd/tM), compared to range of measured values. [Data based on Ref. [27] were evaluated using $\Delta V^{\text{gaseous FP}}/V_0^{\text{matrix}} = \Delta V_b/V_0 + X \cdot F \cdot Y_{Xe} \cdot BU \cdot 3\Omega$ where X is the fraction of gas in dynamic solution and $\Delta V_b/V_0$ is the total fractional bubble swelling (intra + intergranular bubbles), with $\Delta V_b/V_0$ saturating at $\approx$0.025 for $BU > 30$ GWd/tM as per [27]. With bubble swelling it is meant here (and throughout this article) the integral fractional volume of cavities that can be resolved only by transmission (TEM) or scanning electron microscopy (SEM), i.e., with typical sizes $<10^{-9}$–10^{-6} m (see also Ref. [27]). Porosity, i.e., the supplementary term to the matrix swelling in Eq. (4), is referred to as the integral fractional volume of larger cavities (pores) that can be resolved simply by optical microscopy, i.e., with typical sizes $\geqslant 10^{-6}$ m.]

in Eq. (17). By increasing ξ the intergranular bubble density is reduced. Thus the (~20%) gas released to the boundaries is distributed in fewer bubbles of larger size, which results in higher intergranular swelling values. Unfortunately, in contrast with the calculated intragranular bubble densities and sizes that were confronted with experiments (Table 2), the intergranular bubble densities and sizes shown in Table 2 could not be corroborated with experimental results due to, in part, the difficult separation of intergranular and intragranular components in the measured (TEM) data. Thus, this aspect of the model still requires experimental confirmation.

However, perhaps the most important reason for the agreement between the trend of the experimental results (of total swelling) and calculations from the present model (Fig. 3) is the calculated evolution of the bubble size distribution with burn-up, which results in a gradually increasing bubble swelling with with burn-up. This is in contrast to the saturated bubble size distribution as adopted in the analysis of Ref. [27] for burn-ups $\geqslant$ 30 GWd/tM, which leads to relatively high bubble swelling at low burn-ups and partially low values at high burn-ups (see Fig. 3 and its caption).

In general, in an irradiation environment where bubble nucleation, gas-atom diffusion to bubbles, and irradiation-induced re-solution are operative, a differential growth rate between bubbles of different size results in a peaked mono-modal size distribution [28]. The position of the peak in the bubble-size distribution that occurs under these conditions is defined by the balance between diffusion of gas-atoms to bubbles and irradiation-induced re-solution of atoms from bubbles. As more gas is added to the lattice (e.g., due to continued fission), the gas-atom diffusion flux to bubbles increases and the peak shifts to larger bubble sizes and decreases in amplitude, resulting in an increased level of bubble swelling with increased burn-up. The model presented in this section describes the average behaviour of this peak as a function of burn-up.

4. Experimental techniques

4.1. Density determinations

Assuming isotropic conditions, the change of the fuel volume during the irradiation can be monitored

by following the variation of one characteristic dimension of the fuel. Several techniques are available for such measurements. However, all of them are subjected to limitations. If the stack length is measured, e.g., by internal extensometers or by gamma-scanning, the pellet gaps (dishing and cracks) influence the results. On the other hand, if the fuel diameter is considered and measurements are made by external sensors, the cladding creep-down and the radial cracks affect the results. Combination of these latter measurements with optical microscopy determinations of the fuel diameter would exclude the cladding contribution. Nonetheless, computation of the crack widths may still be needed to suppress this contribution to the fuel diameter.

Therefore, the volume variation is mostly determined via density measurements, since these results are independent of the fuel crack patterns and the cladding contributions. The method assumes mass conservation during irradiation and entails determining of the sample density by the Archimedes Principle, i.e. measuring of the sample weight in air and after immersion in a liquid that penetrates the open porosity (water, methanol, monobromobenzene, 1,1,2,2-tetrabromoethane, etc. [6,29]). Usually several pieces of decladded fuel are included in the test with a total weight of about one pellet [29]. Possible systematic errors affecting the results could be the incomplete contribution of the rim porosity if outer pieces are not fully detached from the cladding (upward shift) and insufficient penetration of the open porosity (downward shift) [30].

4.2. Porosity determinations by quantitative metallography

As is evident from Eq. (2) the derivation of matrix swelling data from density measurements requires the determination of the fuel porosity at the burn-ups in question. This is done traditionally by quantitative image analysis of optical or scanning electron microscopy micrographs of sections neighbouring those selected for density measurements [6,8]. If as at burn-ups $<$40 GWd/tM, the porosity of the fuel is homogeneously distributed, it is sufficient to consider a limited number of observations [8]. If, as at higher burn-ups, the porosity of the fuel shows strong gradients (e.g., increasing towards the rim) [7], more numerous observations across the radius and area integration of this data are needed in order to assign a unique porosity value to each average pellet burn-up [30].

The above technique is nonetheless subjected to large errors, which depend on the sample preparation (pore smearing, grain pull-out), the operator (detection threshold, grey scale, feature selection), the magnification selection (compromise between accuracy and representativeness of the measurement) and the azimuthal variation of the features [6,7,30]. Fig. 4 shows the typical variation of the fuel porosity with the pellet radius and burn-up, revealing the different zones with different porosity types that are manifested in the fuels, and the usual spread of the results. As shown with more detail in Fig. 5 for a LWR-fuel with 97 GWd/tM burn-up,

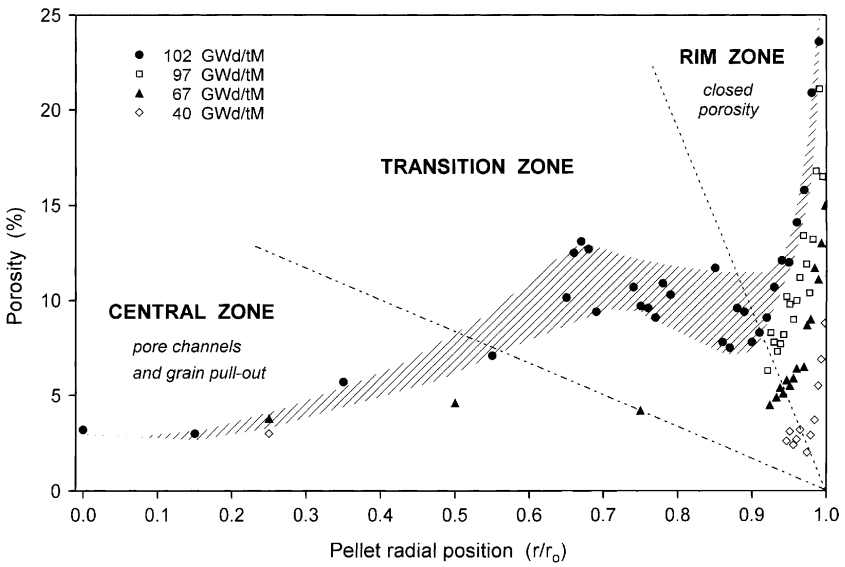

Fig. 4. Variation of the fuel porosity with the pellet radius and burn-up. Central zone with characteristic decorated grains, abundant intergranular pore channels and a marked trend to grain pull-out. Rim zone with characteristic closed porosity and lesser propensity to grain pull-out.

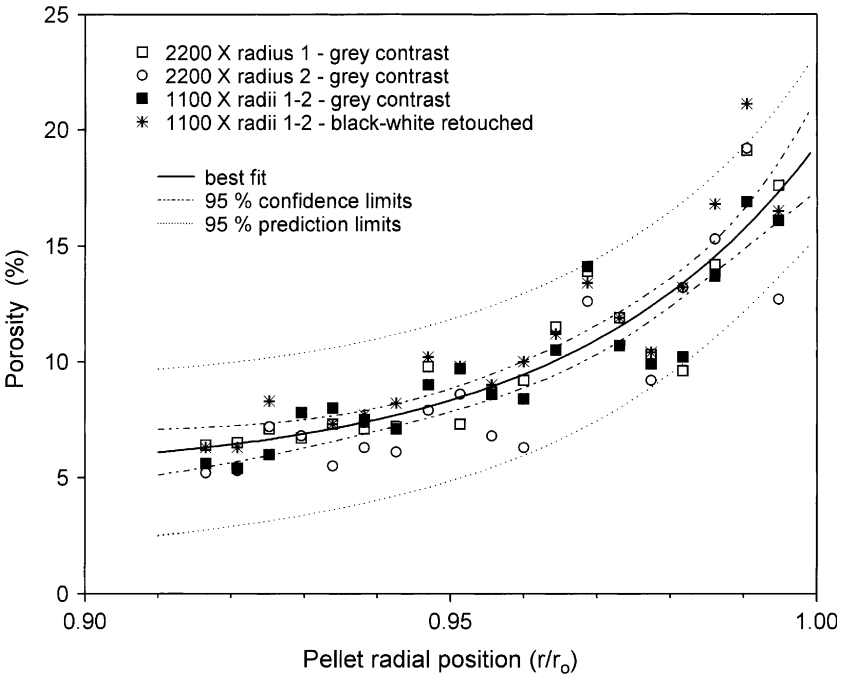

Fig. 5. Scatter of porosity data from quantitative image analysis, considering different micrograph magnifications and contrast levels, and different (azimuthally neighbouring) radii. LWR fuel with 97 GWd/tM average pellet burn-up.

considering the effect of different micrograph contrasts and magnifications and different (azimuthally neighbouring) radii, the error band of these measurements (for the 95% confidence level) cannot be set below ±1–2 vol.%.

4.3. Determination of matrix retained Xe by EPMA

The quantitative determination of the amount of Xe retained in the fuel matrix has been carried out successfully at ITU over the years for a variety of fuel programmes, by application of an electron probe microanalysis (EPMA) technique, which allows quantifying the Xe concentration in the solid by using an antimony standard [31]. The use of the technique specifically for the case of high burn-up LWR-fuels has been thoroughly described in [32,33]. Around 40 data points are used to construct the radial Xe profile, with individual determinations being done characteristically on areas of 3–4 μm in diameter [32]. By checking the specimen current image (electron absorption image) care is taken that the probe beam impinges preferentially on matrix material with the lowest possible contribution from voids (pores) and grain boundary gas bubbles [32].

A correction of the measured Xe-intensity due to the influence of micro-cavities in the matrix is here in a first approach neglected. This is because: (a) bubbles in the nm-range cause only slight modification of the signal (Fig. 4 of Ref. [34]), (b) as shown in Sections 3.2 and 3.3, only a part of the retained gas in the matrix is present in form of bubbles; the rest remaining in dynamic solution. As for the gas potentially stored in the porosity it is for the purpose of this analysis irrelevant, since it does not contribute to the matrix swelling. Similarly to the case of the porosity profiles, area integration of the Xe radial profiles is performed to assign a unique value of retained Xe to a given average pellet burn-up. The uncertainty interval of the measured Xe-concentrations at 95% confidence level (2σ) is typically 0.025 wt.% at a concentration of 0.5 wt.% and 0.05–0.01 wt.% at a concentration of 0.05 wt.% [35].

5. Results

5.1. Density measurements

The relative immersion density results for more than seventy LWR-fuel samples with average burn-ups up to 100 GWd/tM are shown in Fig. 6. The figure shows also the best polynomial fit to the data ($r^2 = 0.931$) and the corresponding 95% confidence limits, indicating an uncertainty of at most ± 1% in the predicted values. It is seen that after the in-pile densification step with saturation at about 15 GWd/tM, the fuel density steadily decreases with burn-up, with a clear increase in slope at burn-ups > 70 GWd/tM. Without any direct physical explanation, for burn-ups in the range 15–100 GWd/tM

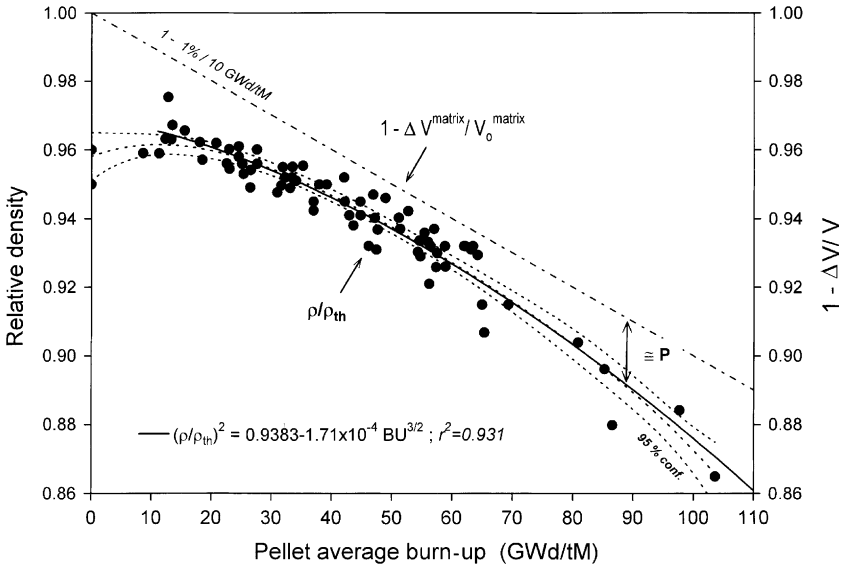

Fig. 6. Measured relative immersion density as a function of the average pellet burn-up.

the density loss is also reasonably reproduced by a simple expression of the type $(\rho/\rho_{th})^2 = (a + b \cdot BU^{3/2})$, with $a = 0.9383$ and $b = 1.71 \times 10^{-4}$ ($r^2 = 0.931$) (Fig. 6). Extrapolation of this trend outside the measured range is, however, uncertain.

Fig. 6 also shows the equivalent density loss attributed to the total matrix swelling $(1 - \Delta V^{matrix}/V_0^{matrix})$ according to the measurements of Ref. [8] (actual range of the determinations: up to 40 GWd/tM). By virtue of Eq. (4), the difference between the density loss due to total matrix swelling and the relative immersion density is approximately equal to the porosity of the fuel. It is seen, therefore, that after the initial in-pile densification step, an approximate constant porosity with a value not larger than 2% would be assigned to the fuels up to the highest burn-ups (Fig. 6). However, despite scatter of the results, the measurements indicate integral porosities clearly above 4% for burn-ups above 70 GWd/tM (Fig. 4). This is the basic contradiction that motivated this work. In the following sections, we demonstrate that this apparent paradox is resolved when the additional void volume required in these cases is provided by the depletion of the fission gases trapped in the fuel matrix.

5.2. Total matrix swelling derived from density–porosity data

Table 3 summarizes the total swelling values and the corresponding average swelling rates obtained for various fuels in the range 40–100 GWd/tM by application of Eqs. (3) and (4). Since the density values (e.g., from Fig. 6) are whole pellet values, the corresponding porosity values (P) considered were the (area) integrals of the radial porosity profiles. The error band assigned to the P values was ±0.015. This error caused an uncertainty of the calculated swelling of ±27–53% (see Table 4). The uncertainty due to the error in the density data is comparatively negligible. Despite the large uncertainty of the results, a glance at Table 4 indicates for burn-ups > 40 GWd/tM a much smaller fuel matrix swelling than previewed at lower burn-ups (0.8% per 10 GWd/tM [5] to 1% per 10 GWd/tM [8]), indeed, nearly a factor of two.

Table 3
Total matrix swelling and swelling rate derived from density and porosity data according to Eqs. (3) and (4)

Burn-up (GWd/tM)	Immersion density (ρ/ρ_{th})	Fractional porosity P	$\Delta V^{matrix}/V_0^{matrix}$ from Eq. (3)	$\Delta V^{matrix}/V_0^{matrix}$ from Eq. (4)	Average total swelling rate (% per 10 GWd/tM) from Eq. (3)
44	0.945	0.027 ± 0.015	0.029 ± 0.016	0.028 ± 0.015	0.66 ± 0.36
67	0.915	0.047 ± 0.015	0.042 ± 0.016	0.038 ± 0.015	0.62 ± 0.25
98	0.884	0.070 ± 0.015	0.052 ± 0.017	0.046 ± 0.015	0.53 ± 0.17
102	0.865	0.087 ± 0.015	0.055 ± 0.017	0.048 ± 0.015	0.54 ± 0.17

The porosity results consist of pellet integral values obtained by (area) integration of radial porosity profiles.

Table 4
Total matrix swelling and swelling rate derived from EPMA results according to Eq. (26)

Burn-up[a] (GWd/tM)	Xe-created (EPMA) (wt.%)	Matrix retained Xe (EPMA) (wt.%)	Retained Xe fraction (EPMA) f^{Xe}	$\Delta V^{matrix}/V_0^{matrix}$ from Eq. (26)	Average total swelling rate (% per 10 GWd/tM)
34	0.47	0.35 ± 0.025	0.75 ± 0.05	0.024 ± 0.001	0.72 ± 0.03
36	0.49	0.48 ± 0.025	0.97 ± 0.05	0.03 ± 0.001	0.84 ± 0.03
42	0.58	0.48 ± 0.025	0.83 ± 0.04	0.032 ± 0.001	0.76 ± 0.02
45	0.62	0.6 ± 0.025	0.97 ± 0.04	0.038 ± 0.001	0.83 ± 0.02
55	0.76	0.6 ± 0.025	0.79 ± 0.03	0.041 ± 0.001	0.74 ± 0.02
59	0.81	0.63 ± 0.025	0.78 ± 0.03	0.043 ± 0.001	0.73 ± 0.02
63	0.87	0.78 ± 0.025	0.9 ± 0.03	0.05 ± 0.001	0.80 ± 0.02
67	0.92	0.72 ± 0.025	0.78 ± 0.03	0.049 ± 0.001	0.73 ± 0.01
83	1.14	0.36 ± 0.025	0.32 ± 0.02	0.04 ± 0.001	0.49 ± 0.01
95	1.31	0.3 ± 0.025	0.23 ± 0.02	0.042 ± 0.001	0.44 ± 0.01
102	1.4	0.22 ± 0.025	0.16 ± 0.02	0.041 ± 0.001	0.40 ± 0.01

The matrix retained Xe concentrations are pellet integral values obtained by (area) integration of radial Xe profiles.

[a] Burn-up: deduced from measured Nd concentration. Other conventions: 1% FIMA = 9.38 GWd/tM (200 MeV/fission). Xe-created (wt.%) = BU(GWd/tM)/9.38 · m_{Xe}/m_{UO_2} · Y_{Xe}, m_{Xe} = average atomic weight of stable Xe isotopes (134), m_{UO_2} = molecular weight UO_2, Y_{Xe} = assumed fission gas yield at high burn-up (0.26).

5.3. Total matrix swelling derived from integrated EPMA-Xe determinations

Considering an average swelling rate by fission gases of about 0.56% per 10 GWd/tM as estimated in Section 3.2 (Van der Waal gas conditions) and derived in Section 3.3, the total matrix swelling can be obtained alternatively from EPMA measurements as follows:

$$\Delta V^{matrix}/V_0^{matrix}(\text{EPMA}) = \text{Burn-up(GWd/tM)}/10 \times (0.0032 + f^{Xe}(\text{EPMA}) \times 0.0056), \quad (26)$$

where f^{Xe} (EPMA) is the total retained Xe fraction in the fuel matrix, which includes both the gas atoms in bubbles and those in dynamic solution.

The total matrix swelling derived from Eq. (26) and the corresponding average swelling rates for a series of LWR-fuels with burn-ups in the range 30–100 GWd/tM are given in Table 4. This also includes the created and retained Xe amounts, and the retained Xe fraction, f^{Xe}. For comparison with results of the previous section (integral data), the retained Xe amounts in Table 4 are pellet integral values as derived from the area integration of the radial Xe-profiles. It is seen that the retained Xe fractions remain at relatively high levels (>0.8) at burn-ups below 70 GWd/tM. However, at higher burn-ups they decrease very rapidly, reaching values <0.2 at ~100 GWd/tM (Table 4). According to Eq. (26) this appreciably reduces the matrix swelling. Thus, in accordance with results in Tables 3, 4 shows that for burn-ups above 8 GWd/tM the average total swelling rates are reduced by more than 50% compared to the lower burn-ups.

The equivalent density loss corresponding to the total matrix swelling values of Tables 3 and 4 are plotted in Fig. 7 as a function of burn-up. For purposes of comparison the relative immersion density curve and the hypothetical density losses assuming only solid fission product swelling [3], or a total matrix swelling according to the values of [5,8] are also shown. Other literature values taken from Ref. [6] are also included in the figure. It is shown that despite the scatter of the results, relatively good agreement exists between all the data up to 60 GWd/tM, suggesting an average total swelling rate of 0.8–1% per 10 GWd/tM, in line with the previous literature values [5,6,8]. However, at higher burn-ups the total matrix swelling becomes progressively reduced, which allows much higher porosity in the fuel to be formed (Eqs. (3) and (4)), in agreement with the observations (Table 3 and Fig. 4).

5.4. Total matrix swelling derived from local EPMA-Xe determinations

In an attempt to extrapolate the previous results to higher burn-ups, Eq. (26) was applied to a set of more than 230 data points corresponding to local EPMA determinations of Xe in the periphery of different LWR-fuels ($r/r_0 > 0.7$), according to a previous compilation (see Fig. 2 in Ref. [31]). These results, covering local burn-ups in the range 14–160 GWd/tM, are plotted in Fig. 8, together with the data of Fig. 7. As a general remark, it is to be noted that at equivalent burn-ups, the matrix swelling calculated from the local EPMA-Xe data lays somewhat below that derived from integrated EPMA-Xe profiles (Fig. 8). This reflects the comparatively smaller retained Xe fraction resulting from the integrated data, which include also Xe depletion in the fuel centre and intermediate regions, of a predominantly thermal origin.

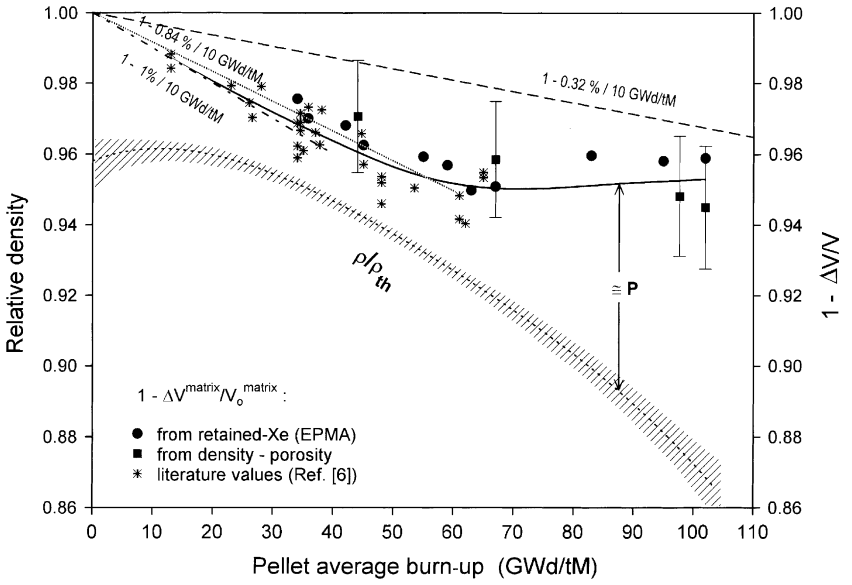

Fig. 7. Total matrix swelling as determined from combined density–porosity results (Eq. (3)) and from retained-XE (EPMA) data (Eq. (26)).

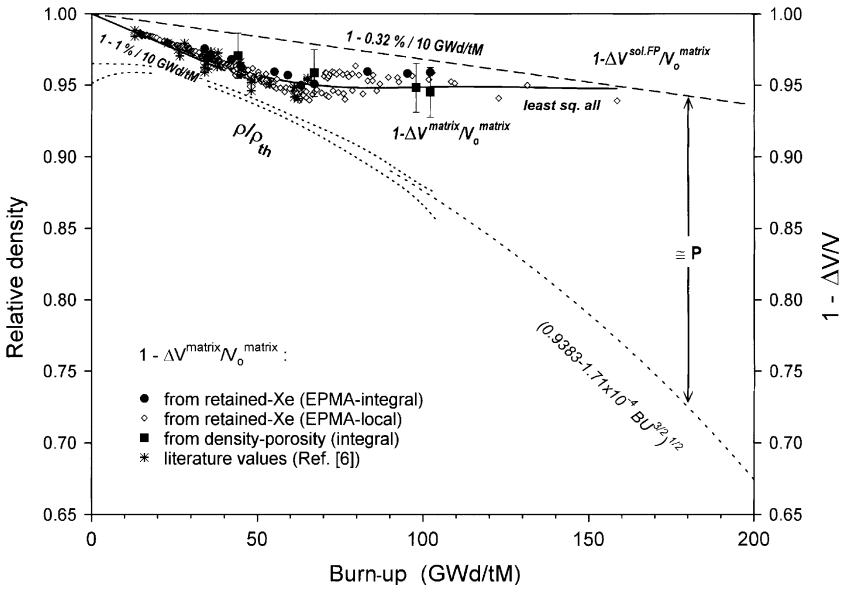

Fig. 8. Total matrix swelling from Eq. (26), using retained matrix-Xe data from local EPMA determinations in the region $0.7 < r/r_0 < 1$ (Data source: Fig. 2 of Ref. [32]). Comparison with integral data.

Despite the above (small) systematic difference, the swelling data from local EPMA-Xe (in reality '$1 - \Delta V^{\text{matrix}}/V_0^{\text{matrix}}$ vs. BU' data) perfectly match the trend indicated in Fig. 7, providing a good basis for the extrapolation to very high burn-ups (Fig. 8). As suggested in the former section (Fig. 5), the data confirm the gradual decrease of the swelling due to fission gases for burn-ups around 60–65 GWd/tM and higher, with probable full disappearance of gas-driven swelling at local burn-ups around 150 GWd/tM and above (Fig. 8). In this very high burn-up range, only solid fission products would govern the matrix swelling.

Although without experimental or theoretical support, the extrapolation of the bulk density curve (ρ/ρ_{th}

vs. *BU*) to the highest burn-up range suggests that peak fuel porosities of the order of 15–20% or larger may be reached (Fig. 8). This is also in agreement with the high local porosities verified in the rim zone of LWR fuels (Fig. 4), for which the maximum local burn-up is approximately twice the average pellet burn-up. The coincidence between the peak porosity values in Fig. 4 and the values suggested in Fig. 8 at the corresponding local burn-ups, is, thus, striking.

6. Discussion

The present work contributes to the clarification of an important question that has emerged since high burn-up LWR-fuels became examined routinely; namely that the measured porosities in the transformed rim zone always appeared too high compared with code predictions. The disagreement was manifested simply upon extrapolation of the available matrix swelling data for low and medium burn-ups, which permitted only fuel porosities of a couple of percents (Fig. 6), in contradiction with the up to 10 times larger measured values (Fig. 4). Even when reduction of the experimental values due to possible operator failures and sample preparation defects was considered, it was never possible to harmonize the rim porosity with the values predicted by the extrapolated swelling. Because of this, the question arose, whether extending burn-ups well beyond the threshold for rim structure formation would cause fuel expansions exceeding the design limits.

However, in line with previous suggestions [5,6], the present results make it clear that in the above volume balance an important component has been ignored; namely, that the depleted fission gas from the fuel matrix no longer contributes to the matrix swelling. At constant density, this provides additional volume for cavity formation (Eqs. (3) and (4)). This is valid for all the gas being thermally or athermally depleted from the fuel matrix, i.e., being released from the central or peripheral regions, and is independent of whether the gas escapes to the plenum or it remains trapped in the porosity.

Accordingly, Figs. 7 and 8 show that for fuel burn-ups greater than 60–65 GWd/tM the matrix swelling becomes visibly reduced. For the curve derived from local EPMA-Xe data ($0.7 < r/r_0 < 1$) (Fig. 8), the transition point is clearly associated with the onset of rim structure formation [7,31]. However, as mentioned in the last section, for the curve derived from integrated data (density–porosity and EPMA-Xe) (Fig. 7), the correlation is not so straightforward, as the data contain also the contributions from the central and intermediate pellet regions. Nevertheless, both curves indicate an unambiguous increasing depletion of fission gases above 60–65 GWd/tM. For the gas in the central and intermediate fuel regions, release to the plenum is most probable [36]; whereas for gas in the rim region, full retention in the (closed) porosity is highly likely [36].

As to the different types of experimental data used to determine the swelling values, the present paper demonstrates the great utility of the EPMA-Xe measurements, due to their definitely smaller error in comparison with the traditional determinations via density and porosity measurements (Eqs. (3) and (4)), particularly due to the inaccuracy of the latter. The method requires, however, knowledge of the solid fission product swelling, and a reliable assignation of the volume expansion due to retained fission gas. This justifies the effort dedicated in this work to the theoretical assessment of this quantity, particularly in view of the partitioning of the retained gas between precipitated bubbles and matrix traps, both with different contributions to the matrix volume expansion.

In Sections 3.2 and 3.3 it has been pointed out that the theoretical estimation of the fuel matrix swelling caused by fission gas requires explicit consideration of the contributions from gas in dynamic solution and from gas in intragranular and intergranular bubbles; gas atoms in dynamic solution occupying 30–50% less volume than gas atoms in bubbles, depending on whether hard sphere model or Van der Waals conditions apply, respectively. Considering a variable partitioning of Xe between bubbles and matrix traps, the model of Section 3.3 permits an average matrix-swelling rate due to fission gases of 0.5–0.6% per 10 GWd/tM to be attributed with reasonable confidence for burn-ups $\leqslant 70$ GWd/tM (Figs. 2 and 3), under the assumption of hard sphere model conditions for Xe [12]. This was possible essentially due to the consideration of evolving bubble size distributions with burn-up, and due to the resulting important contribution of intergranular bubbles to swelling. Fortuitously, the cited range of values fully comprise the matrix expansion previously calculated for Xe under assumption of Van der Waals EOS conditions and neglecting radiation-induced re-solution of bubbles (i.e., 8.5×10^{-23} cm^3/atom [3,5], 0.56% per 10 GWd/tM) (Section 3.2), which facilitates the evaluation of experiments (see Section 5.3), and is in line with the previous recommendation in [5].

In the present work, no variation of the matrix swelling caused by solid fission products was considered. However, modifications of the fuel-gap chemistry could occur at high burn-ups, for instance due to oxygen uptake by formation of cladding oxide layers and gap bonding compounds [6], which could alter the character and volume demand of the precipitate phases. Related with this, it is to be noted that due to the assumed increased Mo-metal precipitation under possible oxygen drop above ~60 GWd/tM, the so-called solid swelling has been proposed to reach its maximum at this burn-up [6]. If confirmed, this effect would allow even more fuel volume to be replaced by porosity than described

in this paper. Additional experimental evidence to confirm this hypothesis is needed.

7. Conclusions

A critical analysis of fuel density, porosity and retained Xe-concentration (EPMA) data of LWR-fuels with burn-ups of 40–100 GWd/tM leads to the conclustion that at burn-ups $\geqslant$ 60 GWd/tM a reduction of the fuel matrix swelling rate occurs, changing gradually from $\approx$1% per 10 GWd/tM to $\approx$0.3% per 10 GWd/tM. The extrapolation of the data indicates that the latter value, representing the matrix expansion due only to solid fission products precipitation, would be reached at local pellet burn-ups of roughly 160 GWd/tM. This effect is due to the progressive release of fission gas from the fuel matrix by thermal or athermal processes, which causes matrix contraction. Owing to volume conservation, the free space left by the depleted gases is replaced by porosity.

References

[1] R.C. Daniel, M.L. Bleiberg, H.B. Meiran, W. Yeniscavich, Report WAP-263, 1962.
[2] F. Anselin, USAEC Report GEAP-5583, General Electric, 1969.
[3] D.R. Olander, Fundamental Aspects of Nuclear Reactor Fuel Elements, Energy Research and Development Administration, TID-26711-P1, 1976.
[4] J. Spino, D. Papaioannou, J. Nucl. Mater. 281 (2000) 146.
[5] Scientific Issues of Fuel Behaviour, Chapter 3, Fission Product Swelling, OECD-NEA, ISBN 92-64-14420-X, January 1995, p. 22.
[6] D. Schrire, A. Kindlund, P. Ekberg, OECD Halden Reactor Project, Enlarged Halden Programme Group Meeting on High Burn-up Fuel Performance, Safety and Reliability and Degradation of In-Core Materials and Water Chemistry Effects, vol. I, Lillehammer, Norway, 15–20 March 1998, HPR-349.
[7] J. Spino, K. Vennix, M. Coquerelle, J. Nucl. Mater. 231 (1996) 179.
[8] H. Assmann, R. Manzel, J. Nucl. Mater. 68 (1977) 360.
[9] H. Zimmermann, J. Nucl. Mater. 75 (1978) 154.
[10] D.G. Franklin, J.T.A. Roberts, C.-Y. Li, J. Nucl. Mater. 125 (1984) 96.
[11] H. Devold, OECD Halden Reactor, Report HWR-252, 1990.
[12] C. Ronchi, J. Nucl. Mater. 96 (1981) 314.
[13] J.A. Turnbull, J. Nucl. Mater. 38 (1971) 203.
[14] J. Rest, J. Nucl. Mater 150 (1987) 203.
[15] J. Rest, J. Nucl. Mater 168 (1989) 243.
[16] M.V. Speight, Nucl. Sci. Eng. 37 (1969) 180.
[17] M.H. Wood, K.L. Kear, J. Nucl. Mater 118 (1983) 320.
[18] N. Nakae, T. Kirihara, S. Nasu, J. Nucl. Mater. 74 (1978) 1.
[19] J. Rest, J. Nucl. Mater 321 (2003) 305.
[20] Hj. Matzke, Nucl. Appl. 2 (1966) 131.
[21] Hj. Matzke, J. Nucl. Mater. 21 (1967) 190.
[22] M.O. Marlow, A.I. Kaznoff, in: Proceedings of International Conference on Nuclear Fuel Performance, British Nuclear Energy Society, London, 1973.
[23] Hj. Matzke, Radiat. Eff. 53 (1980) 219.
[24] K. Nogita, K. Une, Nucl. Instrum. and Meth. B 91 (1994) 301.
[25] K. Nogita, K. Une, J. Nucl. Mater. 226 (1995) 302.
[26] A.C.S. Sabioni, W.B. Ferraz, F. Millot, J. Nucl. Mater. 278 (2000) 364.
[27] C. Ronchi, M. Scheindlin, D. Staicu, M. Kinoshita, J. Nucl. Mater. 327 (2004) 58.
[28] M.V. Speight, J. Nucl. Mater. 38 (1971) 236.
[29] E. Toscano, ITU, private communication, 2004.
[30] J. Spino, D. Papaioannou, I. Ray, D. Baron, Fission Gas Behaviour in Water Reactor Fuels, Seminar Proceedings, Cadarache, France, 26–29 September 2000, Report NEA/OECD, NEA # 03053, 2002, p. 247 (ISBN 92-64-19715-X).
[31] C.T. Walker, J. Nucl. Mater. 80 (1979) 190.
[32] C.T. Walker, J. Nucl. Mater. 275 (1999) 56.
[33] R. Manzel, C.T. Walker, J. Nucl. Mater. 301 (2002) 170.
[34] C. Ronchi, C.T. Walker, J. Phys. D 13 (1980) 2175.
[35] M. Mogensen, C. Bagger, C.T. Walker, J. Nucl. Mater. 199 (1993) 85.
[36] J. Spino, D. Papaioannou, J.-P. Glatz, J. Nucl. Mater. 328 (2004) 67.